

Dielectric permittivity of ultrathin PbTiO_3 nanowires from first principles

G. Pilania · R. Ramprasad

Received: 3 January 2012 / Accepted: 12 March 2012
© Springer Science+Business Media, LLC 2012

Abstract We propose an efficient method to compute the dielectric permittivity of nanostructures by combining first principles density functional perturbation theory with effective medium theory. Specifically, ultrathin axially symmetric ferroelectric PbTiO_3 nanowires are considered. As established previously by Pilania and Ramprasad (Phys Rev B 82:155442, 2010), (4×4) PbO-terminated nanowire and (4×4) TiO_2 -terminated nanowire display, respectively, a uniform axial and a vortex polarization in their ground state configurations (the latter with a non-zero axial toroidal moment). Both nanowires, regardless of the lateral surface termination, display a significantly larger dielectric constant value along the axial direction, and diminished values along the off-axis directions, as compared to the corresponding bulk values. Our results further suggest that the nanowires with unconventional vortex-type polarization states are expected to have an increased dielectric response as compared to those with conventional uniform axial polarization. The method proposed here is quite general and readily extendable to other zero-, one-, and two-dimensional nanostructures.

Introduction

Due to an attractive combination of tunable ferroelectric and dielectric properties, ferroelectric nanostructures have

an immense potential for many technological applications [1–11]. The delicate phenomenon of ferroelectricity—defined as the presence of spontaneous and switchable lattice polarization—is strongly modulated by electrical, physical, and mechanical boundary conditions [12–15]. As a result, the polarization and dielectric response of ferroelectric nanostructures has remained uncertain. For instance, the absence of adequate screening and uncompensated surface charges in nanostructures result in depolarizing fields. Below a critical length scale, it is believed that the depolarizing fields may lead to vanishing polarization along the reduced dimension, and consequently, to the suppression of ferroelectric phase transitions [16].

While the elimination of ferroelectricity due to reduced dimensionality may be one possibility, it has been conjectured that a second possibility is the formation of closure or vortex electric dipole configurations. This expectation has been motivated by effective Hamiltonian [17–20] and first principles simulations [21–26], indirect experimental data [27, 28], and analogy to ferromagnetic nanostructures [29–31]. A vortex or closure dipole configuration is characterized by a non-rectilinear arrangement of local polarization vectors, and could lead to a non-zero net polarization along the reduced dimensions. Such closure domains thus allow for the elimination of the depolarizing fields while still satisfying the propensity of the system to be polarized (albeit locally). In fact, our own recent parameter-free first principles computations have shown the existence of such polarization ordering in PbTiO_3 [21] and BaTiO_3 [22] nanowires. The critical size for the genesis of a vortex polarization state in these nanowires was found to be 16 Å at zero temperature. Figure 1 captures the essence of our findings for the PbTiO_3 nanowires, and shows that the (4×4) PbO-terminated nanowire displays a pure axial polarization in its ground state, while the

G. Pilania · R. Ramprasad (✉)
Chemical, Materials, and Biomolecular Engineering,
Institute of Materials Science, University of Connecticut,
Storrs, CT 06269, USA
e-mail: rampi@ims.uconn.edu

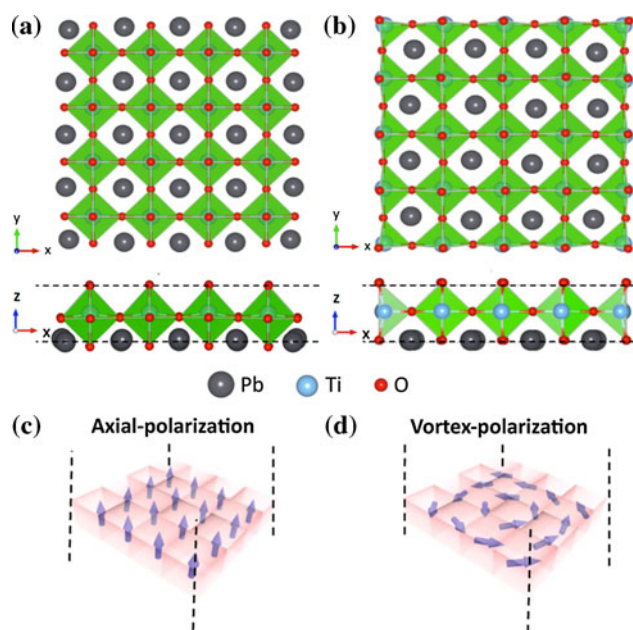


Fig. 1 Top and side views of **a** (4×4) PbO-terminated PbTiO₃ nanowire and **b** (4×4) TiO₂-terminated PbTiO₃ nanowire investigated in this study. **c** Rectilinear axial and **d** non-rectilinear vortex ground state polarization configurations, predicted for the PbO- and TiO₂-terminated wires, respectively [21]. The *arrows* in the two *bottom panels* indicate the direction of the dipole moments in the primitive unit cells

(4×4) TiO₂-terminated nanowire allows for the occurrence of a non-rectilinear vortex state.

Although polarization ordering phenomena in ferroelectric nanostructures have been addressed in the past, the dielectric constant of such nanostructures—an important property in its own right—has not been determined from first principles to-date. In this contribution, we address the dielectric response of PbTiO₃ nanowires, both in the presence of rectilinear as well as non-rectilinear polarization states. While the computation of the dielectric constant of bulk materials is currently straightforward [32, 33], that for nanostructures which contain surfaces is non-trivial. Important advancements have indeed been made in the latter area in the recent past [34–44]. The difference in the dielectric response of the surface atoms relative to the atoms in the bulk, and the proper definition of the volume occupied by the system have been challenges. In this study, we employ density functional perturbation theory (DFPT) combined with effective medium theory to directly obtain the dielectric permittivity of PbTiO₃ nanowires. The method is readily extendable to other materials with different levels of dimensionality.

The rest of the paper is organized as follows. In “**Theoretical details**” section, we describe the computational methods and model details employed here to calculate the dielectric constants of nanowires. In “**Results and discussion**” section,

we report and discuss the dielectric properties of PbTiO₃ nanowires. Finally, the article is concluded.

Theoretical details

Computational details

Ab initio calculations based on the density functional theory (DFT) [45, 46] were carried out using the Vienna ab initio simulation package (VASP) [47, 48]. The electronic wave functions were expanded in plane-waves up to a cut-off energy of 500 eV. The electron–ion interaction was described by the projector-augmented wave (PAW) potentials [49, 50], which explicitly included the Pb 5*d*, 6*s*, and 6*p*, the Ti 3*s*, 3*p*, 3*d*, and 4*s*, and the O 2*s* and 2*p* electrons in the valence states. To evaluate the exchange–correlation energy, we employed the local density approximation (LDA) of the Ceperley–Alder form [51], because the generalized gradient approximation (GGA) significantly overestimates both the equilibrium volume and the *c/a* ratio of PbTiO₃ [52]. We use a $1 \times 1 \times 6$ Monkhorst-Pack sampling of the Brillouin-zone integrations [53] for the nanowires considered in this study. The convergence of the present calculations with respect to *k*-point mesh and plane-waves cut-off energy have been checked thoroughly. In this study, free standing, infinitely long and axially symmetric (4×4) PbO- and TiO₂-terminated nanowires were modeled using periodic boundary conditions with their axis along the [001] direction (cf. Fig. 1a, b). Note that irrespective of the nanowire sidewall termination (i.e., PbO- or TiO₂-termination), both the wires have an alternate stacking of PbO and TiO₂ planes along the axial direction. A vacuum of at least 12 Å was used to prevent any unphysical interactions between a wire and its periodic images along the transverse directions.

The electronic structure, ground state geometry, and polarization configurations for the PbTiO₃ nanowires considered here have been discussed in detail in our previous study [21]. While both the (4×4) PbO- and (4×4) TiO₂-terminated PbTiO₃ nanowires show ferroelectric instability, the nature of the ferroelectric polarization revealed by the ground state configurations in the two nanowires is quite different. As shown in Fig. 1c, the (4×4) PbO-terminated wire bears a uniform axial polarization ($90.53 \mu\text{C}/\text{cm}^2$) comparable to that of bulk PbTiO₃ ($85 \mu\text{C}/\text{cm}^2$ at the room temperature [54]). The ground state of the (4×4) TiO₂-terminated nanowire turns out to be a pure vortex state, with the local polarization vector forming a closed loop in the plane normal to the axis, as depicted in Fig. 1d. This nanowire shows a zero net polarization along *x*, *y*, and *z* directions, and a non-zero moment of polarization along the axial direction.

Procedure to compute dielectric permittivity

The dielectric constant of the nanowires in the supercell geometry was evaluated using the DFPT [32, 33]. We note though that the dielectric constant provided by DFPT includes the contributions from the nanowire as well as the intervening vacuum region of the supercell. Treating the supercell as a vacuum-nanowire composite and using the appropriate formulae from effective dielectric medium theory, as described below, enables us to further extract the permittivity (both optical and static contributions) of just the nanowires.

According to the Maxwell–Garnett equation, which can be considered as an extension of the Clausius–Mossotti relation, the principal components of dielectric permittivity of a vacuum-filler composite (ϵ_{ii}) containing a volume fraction η_v of polarizable fillers (i.e., nanowires, in the present case) with dielectric permittivity ($\epsilon_{ii}^{\text{wire}}$) can be written as [55]

$$\frac{\epsilon_{ii} - 1}{1 + (\epsilon_{ii} - 1)P_i} = \eta_v \frac{\epsilon_{ii}^{\text{wire}} - 1}{1 + (\epsilon_{ii}^{\text{wire}} - 1)P_i} \tag{1}$$

where i ($=x, y, z$) represents the cartesian axes and the P_i are the geometry-dependent depolarizing factors, which are tabulated in the literature [56–58]. For the case at hand, assuming that the nanowires are oriented along the z direction, $P_x = P_y = 0.5$, and $P_z = 0$. This leads to the following relations for the off-axis and axial components of the dielectric permittivity:

$$\frac{\epsilon_{xx} - 1}{\epsilon_{xx} + 1} = \eta_v \frac{\epsilon_{xx}^{\text{wire}} - 1}{\epsilon_{xx}^{\text{wire}} + 1} \tag{2}$$

$$\epsilon_{zz} = \eta_v (\epsilon_{zz}^{\text{wire}} - 1) + 1 \tag{3}$$

$\epsilon_{ii}^{\text{wire}}$ may be determined from the above equations via a knowledge of η_v , and the ϵ_{ii} values obtained from the DFPT calculations. Determination of η_v , however, is non-trivial. Owing to the slowly decaying nature of the charge density itself, we use the induced screening charge density to quantify the volume occupied by the nanowire (and hence, η_v). To do this, an electric field of strength $\pm 0.01 \text{ V/\AA}$ was applied along the off-axis (non-periodic) direction for each of the wires in their ground state configurations, and the field-induced total charge density (i.e., the screening charge density) was calculated as the difference between the total charge density due to the oppositely directed fields. The calculated planar average of the screening charge distribution ($\rho^{\text{scr}}(x)$) is shown in Fig. 2 for each of the two nanowires. From Fig. 2, we can see that the screening charge piles up at the surface of the nanowires and is mainly confined above the surface atoms. These surface charges are responsible for the screening of

the external applied electric field and therefore justify using the screening charge density as a criterion to place a boundary between the nanowires and the vacuum region of the supercell. Specifically, the size of the wire along the off-axis direction was taken to be the distance between the two points where the linear extrapolation of the sharp drop in the outermost peak of the screening charge density goes to zero (as shown in Fig. 2), omitting the slowly decaying tail of the screening charge density.

For each of the nanowires, we perform three different DFPT calculations by varying the supercell volume, and hence, the volume fraction, η_v . More specifically, the supercell dimension along the x and y directions was kept fixed at 28, 32, and 36 Å in the three separate calculations, while the supercell dimension along the z direction was always kept fixed at the corresponding relaxed (or equilibrium) c lattice parameter of the nanowire. The volume occupied by each nanowire was then determined using the off-axis dimension, determined as discussed above, and the axial periodic repeat distance. A plot of the left-hand side expression of Eqs. 2 and 3 versus η_v should lead to a linear relationship, with the slope providing the $\epsilon_{ii}^{\text{wire}}$ value.

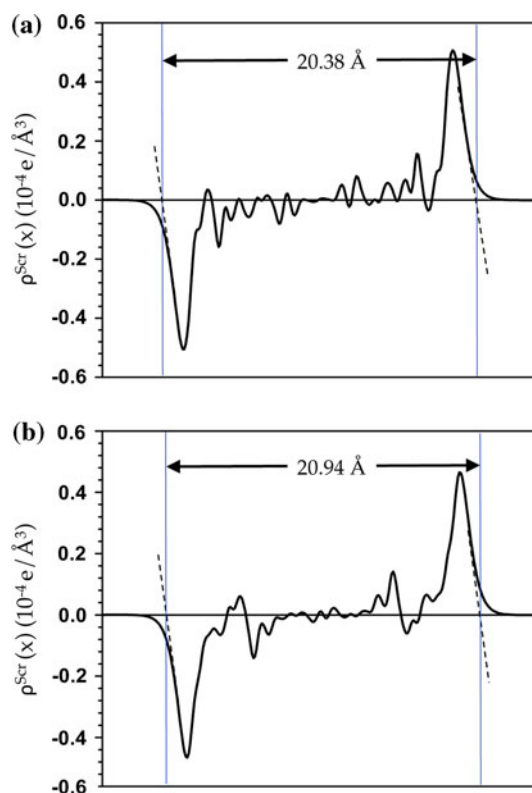


Fig. 2 Planar-averaged screening charge distribution of **a** PbO-terminated PbTiO₃ nanowire and **b** TiO₂-terminated PbTiO₃ nanowire along the x axis, calculated for an electric field of $\pm 0.01 \text{ V/\AA}$. The estimated size of the each nanowire is also indicated in the respective panels

Results and discussion

As a validation of the computational methodology adopted in this study, we first calculate the optical (the high frequency, or the electronic) and static (the low frequency, or the ionic plus electronic) dielectric permittivities of bulk PbTiO₃ in both the high temperature cubic and the ground state tetragonal phases. Our results are presented in Table 1. The calculated optical dielectric permittivity of the cubic PbTiO₃ is in excellent agreement with the corresponding experimental [59, 60] and theoretical [61] results reported in the literature. Unlike the cubic phase, the tetragonal PbTiO₃ has two principal dielectric constants. Based on Raman scattering measurements of clamped single domain PbTiO₃ crystals, Frey and Silberman [63] have reported high frequency dielectric constant values of $\epsilon_{zz}^{\infty, \text{bulk}} = 7.211$ and $\epsilon_{xx}^{\infty, \text{bulk}} = 7.270$ along the tetragonal *c* and *a* axes, respectively, and static dielectric constant values of $\epsilon_{zz}^{0, \text{bulk}} = 30.4$ and $\epsilon_{xx}^{0, \text{bulk}} = 125.6$. Similar values, have also been reported by Fontana et al. [64] ($\epsilon_{zz}^{0, \text{bulk}} = 32$ and $\epsilon_{xx}^{0, \text{bulk}} = 100$) and Foster et al. [65] ($\epsilon_{zz}^{0, \text{bulk}} = 28.6$ and $\epsilon_{xx}^{0, \text{bulk}} = 106.9$). On the theoretical side, the optical and static dielectric constant values of 7.24 and 36.4, respectively, along the *c* axis have recently been reported by Yu et al. [41] based on linear response calculations. Our calculated values for the tetragonal as well as for the cubic phases of PbTiO₃ (cf. Table 1) show an overall good agreement with all these previously reported results.

Next we move our discussion to the dielectric permittivity of the nanowires. The results of our calculations for various supercell sizes, i.e., various nanowire volume

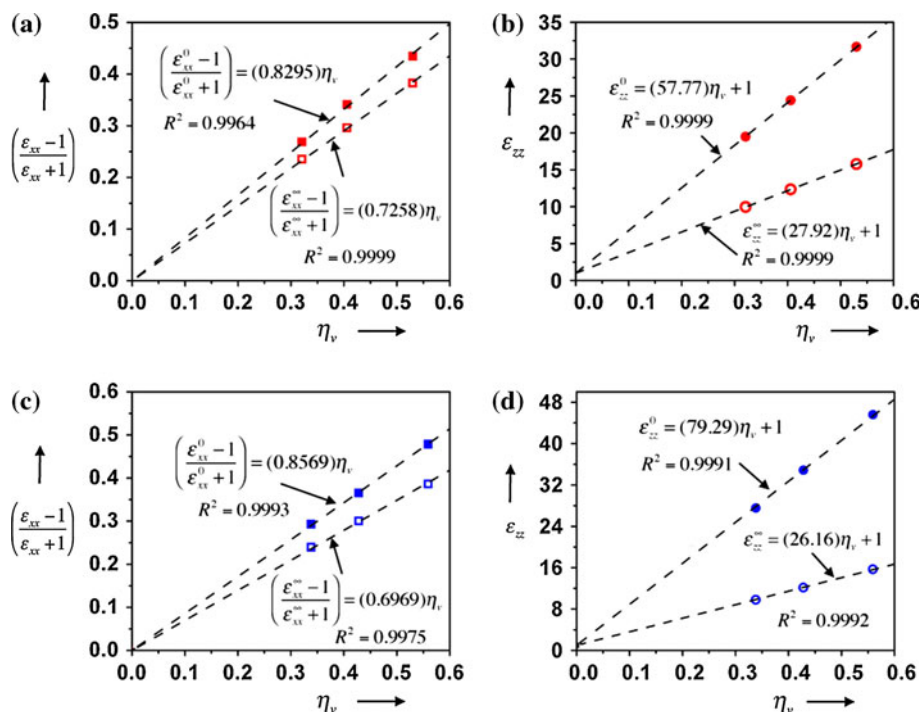
fractions η_v , are plotted in Fig. 3a, b for the (4 × 4) PbO-terminated nanowire and Fig. 3c, d for the (4 × 4) TiO₂-terminated nanowire. It can be seen that a linear behavior as expected from the Eqs. 2 and 3 is indeed followed between the term on the left-hand side of those equations and η_v , with the slope allowing us to calculate dielectric permittivity contribution due to the nanowires alone. The calculated optical and static dielectric permittivity values for the two nanowires are reported in Table 1 and Fig. 4.

Several important observations can be made from Table 1 and Fig. 4. First, we note that the dielectric constant of the TiO₂-terminated nanowire (bearing a vortex polarization configuration) is higher than that of the PbO-terminated nanowire (displaying axial polarization) in both the axial and off-axis directions. Second, the off-axis component of the optical and static dielectric constants of both the nanowires are significantly smaller than the corresponding values of the bulk material in the same direction. This can be attributed to the depolarizing fields which severely limit the net polarizability of the wires along non-periodic directions. Moreover, the difference in the off-axis dielectric constant of the two differently terminated nanowires is minimal (although the ground state polarization states are very different)—the reason again being that any differences in the dielectric response is “quenched” by depolarizing fields. Third, the axial components of the dielectric constant of the nanowires are markedly larger than those of the corresponding bulk in the same direction. Interestingly, in the case of the PbO-terminated nanowire, this increase is largely due to the optical contribution to the dielectric constant, and the ionic contribution is roughly the

Table 1 Calculated optical and static dielectric constants of PbTiO₃ bulk in both the cubic and tetragonal phases ($\epsilon_{ii}^{\infty, \text{bulk}}$ and $\epsilon_{ii}^{0, \text{bulk}}$, respectively) and nanowires ($\epsilon_{ii}^{\infty, \text{wire}}$ and $\epsilon_{ii}^{0, \text{wire}}$, respectively)

Bulk	Optical		Static	
	$\epsilon_{xx}^{\infty, \text{bulk}}$	$\epsilon_{zz}^{\infty, \text{bulk}}$	$\epsilon_{xx}^{0, \text{bulk}}$	$\epsilon_{zz}^{0, \text{bulk}}$
Cubic				
This study	8.85	8.85	23.26	23.26
Other (experiments)	8.70 [59, 60]	8.70 [59, 60]	–	–
Other (theory)	8.24 [61]	8.24 [61]	–	–
Tetragonal				
This study	8.00	7.47	170.95	33.73
Other (experiments)	7.27 [62]	7.20 [62]	100 [64]	32 [64]
	7.27 [63]	7.21 [63]	125.6 [63]	30.4 [63]
	–	–	106.9 [65]	28.6 [65]
Other (theory)	–	7.24 [41]	–	36.4 [41]
Nanowires				
	$\epsilon_{xx}^{\infty, \text{wire}}$	$\epsilon_{zz}^{\infty, \text{wire}}$	$\epsilon_{xx}^{0, \text{wire}}$	$\epsilon_{zz}^{0, \text{wire}}$
(4 × 4) PbO-terminated	6.29	28.92	10.73	58.77
(4 × 4) TiO ₂ -terminated	5.60	27.16	12.98	80.29

Fig. 3 Linear variations of $(\epsilon_{xx} - 1)/(\epsilon_{xx} + 1)$ (a) and ϵ_{zz} (b) as a function of the fractional volume η_v ($V_{\text{wire}}/V_{\text{supercell}}$) for the PbO-terminated PbTiO₃ nanowires, as dictated by the 2D Maxwell-Garnett mixing rule (cf. Eq. 2) and the linear mixing rule (cf. Eq. 3), respectively. **c, d** are same as the (a) and (b) but for the TiO₂-terminated nanowire. *Open and closed symbols* in each of the *panels* have been used for the optical and static dielectric permittivity components, respectively



same as in the bulk material (we note that the ionic contribution is just the difference between the static and optical contributions). The behavior of the ionic contribution is consistent with the fact that both in the bulk and in the PbO-terminated nanowire, the polarization state is identical. In the case of the TiO₂-terminated nanowire (which bears a vortex polarization state), both the electronic (or optical) and the ionic contributions to the dielectric constant are significantly higher than that of the corresponding bulk. The enhancement of the ionic contribution can be explained by observing that, unlike the bulk

material, the nanowire bears no polarization along the axial direction to begin with, and is hence polarizable along that direction far more than the bulk.

While we may explain the behavior of the ionic contributions to the dielectric constant in terms of depolarizing fields and the tendency for polarization along periodic dimensions, the behavior of the optical (or electronic) part of the dielectric constant is puzzling. We note that the presence of mid-gap surface states may also lead to an increased dielectric response through an effective narrowing of the electronic gap. To further confirm that the predicted enhanced dielectric response in the PbTiO₃ nanowires is indeed an intrinsic property of the material at reduced dimensionality and is not due to the mid-gap states arising as a result of the coordinative unsaturation at the lateral surfaces of the nanowires, we analyze the density of states (DOS) of the two nanowires. In this analysis, the total DOS is decomposed in terms of the contributions due to the core and shell regions, of the two nanowires. For each of the two wires, the central four PbTiO₃ units constitute the core region while the 12 peripheral units form the shell region, as indicated schematically in the upper panels in Fig. 5. The core (in blue) and shell (in red) decomposed density of states are plotted in the lower panels for the PbO- and TiO₂-terminated nanowires, respectively. The bulk DOS (black-dashed line) is also included in each of the two figures for comparison. Our analysis clearly reveals clean electronic bandgaps for both the nanowires, which also translate to the thermodynamic and chemical stability of these systems. The absence of any

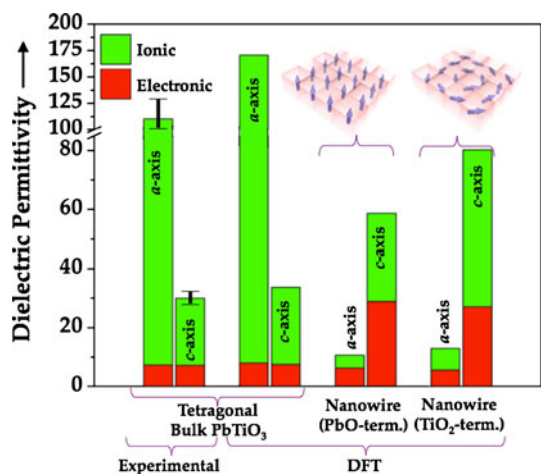
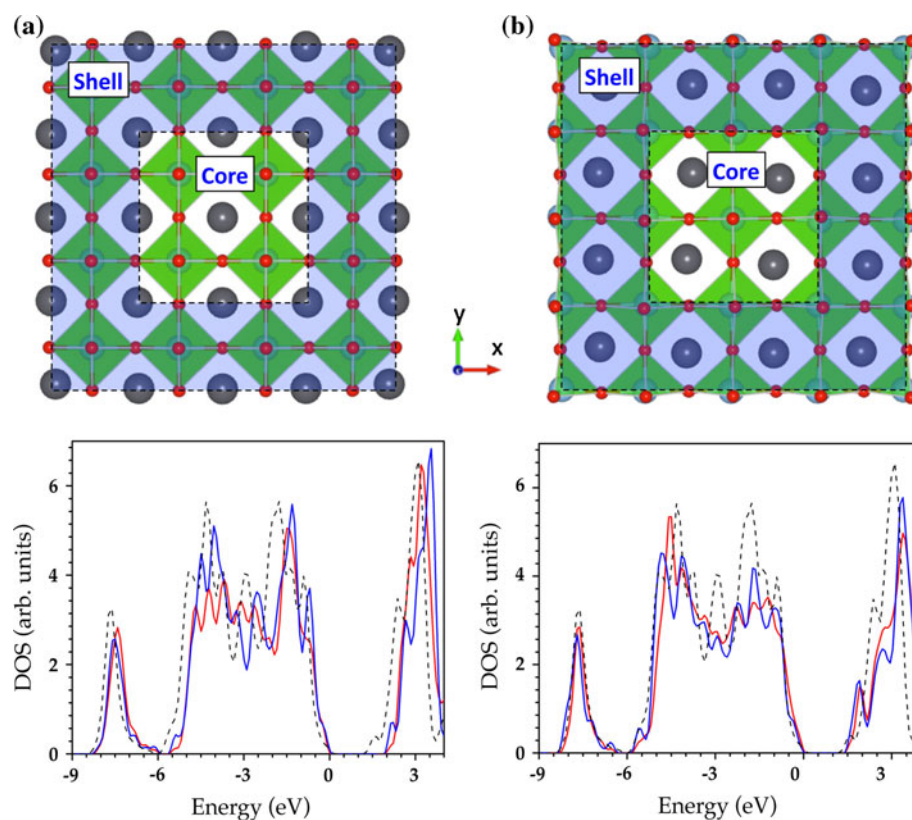


Fig. 4 Calculated dielectric permittivities of PbTiO₃ bulk (tetragonal phase) and the two nanowires. The corresponding experimental results for the bulk PbTiO₃ are also included for comparison [ref 62–65]

Fig. 5 Core- and shell-decomposed DOS for the **a** (4×4) PbO-terminated nanowire and **b** (4×4) TiO₂-terminated nanowire, in each case normalized to a single PbTiO₃ unit. The core (four PbTiO₃ units at the center) and shell (12 peripheral PbTiO₃ units) regions used in the DOS decomposition for the two nanowires are shown schematically in the *upper part* of each of the *panels*. In each of the DOS plots, *blue* and *red* lines indicate the contributions due to the core and shell regions, respectively. Bulk DOS for the tetragonal PbTiO₃ is also shown for comparison in each of the two plots (*dashed line*) (Color figure online)



mid-gap, or gap-narrowing features indicates that the observed dielectric response is primarily due to reduced dimensionality and the unusual polarization states inherent to these nanowires.

Conclusions

In conclusion, we have determined the dielectric permittivity of ultrathin PbTiO₃ nanowires employing a hybrid approach that combines first principles DFPT calculations with effective medium theory. The choice of PbTiO₃ nanowires as a model system was motivated by *both* a strong intrinsic tendency for polarization exhibited by bulk PbTiO₃ and the presence of conventional (axial) and unconventional (vortex-type) polarization configurations in ultrathin PbTiO₃ nanowires. Our calculated dielectric constants of bulk cubic and tetragonal PbTiO₃ agree well with previous experimental and theoretical work. Going from bulk to ultrathin nanowires, our prediction of a decrease in the dielectric permittivities along the off-axis directions is attributed to the depolarizing fields along those non-periodic directions. On the other hand, along the axial direction, the dielectric permittivity shows a significant enhancement over the corresponding bulk value. Moreover, we predict a higher dielectric constant along the axial direction for the TiO₂-terminated nanowire with

ground state vortex polarization configuration as compared to the PbO-terminated nanowire which displays a conventional rectilinear polarization along the axis. This prediction is consistent with the well-known notion that the dielectric response is higher along a high symmetry direction along which polarization is originally absent. Furthermore, the core-shell-decomposed DOS analysis shows the absence of any bandgap narrowing features, thereby pointing to the chemical and thermodynamic stability of these systems.

While we have demonstrated the applicability of the presented method for a specific case of PbTiO₃ nanowires, this simple procedure has a broader appeal, as it can be readily extended to study other systems as well as other situations with varying levels of dimensionality.

Acknowledgements The authors would like to acknowledge financial support of this study by a grant from the Office of Naval Research. Computational support was provided through a National Science Foundation Teragrid Resource Allocation.

References

1. Park BH, Kang BS, Bu SD, Noh TW, Lee J, Jo W (1999) Nature (London) 401:682
2. Velu G, Legrand C, Tharaud O, Chapoton A, Remiens D, Horowitz G (2001) Appl Phys Lett 79:659
3. Han S, Liu X, Han J-P, Zhou C (2003) Appl Phys A 77:873

4. Han J, Ma TP (1998) *Appl Phys Lett* 72:1185
5. Auciello O, Scott JF, Ramesh R (1998) *Phys Today* 51:22
6. Kim P, Jones SC, Hotchkiss PJ, Haddock JN, Kippelen B, Marder SR, Perry JW (2007) *Adv Mater* 19:1001
7. Schroeder R, Majewski LA, Grell M (2005) *Adv Mater* 17:1535
8. Cao Y, Irwin PC, Younsi K (2004) *IEEE Trans Dielectr Electr Insul* 11:797
9. Bai Y, Cheng Z-Y, Bharti V, Xu HS, Zhang QM (2000) *Appl Phys Lett* 76:3804
10. Hippel AV (ed) (1954) *Dielectric materials and applications*. Technology Press of MIT, Cambridge
11. Scott JF (2000) *Ferroelectric memories*. Springer, Berlin
12. Lines ME, Glass AM (1977) *Principles and applications of ferroelectrics and related materials*. Clarendon, Oxford
13. Rabe, K, Ahn, ChH, Triscone, J-M (eds) (2007) *Physics of ferroelectrics: a modern perspective*. Springer, Berlin
14. Junquera J, Ghosez Ph (2008) *J Comput Theor Nanosci* 5:2071
15. Rabe KM (2005) *Curr Opin Solid State Mater Sci* 9:122
16. Junquera J, Ghosez Ph (2003) *Nature (London)* 422:506
17. Fu H, Bellaiche L (2003) *Phys Rev Lett* 91:257601
18. Naumov I, Bellaiche L, Fu H (2004) *Nature* 432:737
19. Ponomareva I, Naumov I, Kornev I, Fu H, Bellaiche L (2005) *Curr Opin Solid State Mater Sci* 9:114
20. Prosandeev S, Bellaiche L (2007) *Phys Rev B* 75:094102
21. Pilania G, Ramprasad R (2010) *Phys Rev B* 82:155442
22. Pilania G, Alpay SP, Ramprasad R (2009) *Phys Rev B* 80:014113
23. Durgun E, Ghosez Ph, Shaltaf R, Gonze X, Raty J-Y (2009) *Phys Rev Lett* 103:247601
24. Aguado-Puente P, Junquera J (2008) *Phys Rev Lett* 100:177601
25. Shimada T, Tomoda S, Kitamura T (2010) *Phys Rev B* 81:144116
26. Shimada T, Wang X, Tomoda S, Marton P, Elsässer C, Kitamura T (2011) *Phys Rev B* 83:094121
27. Gruverman A, Wu D, Fan H-J, Vrejoiu I, Alexe M, Harrison RJ, Scott JF (2008) *J Phys: Condens Matter* 20:342201
28. Thompson C, Fong DD, Wang RV, Jiang F, Streiffer SK, Latifi K, Eastman JA, Fuoss PH, Stephenson GB (2008) *Appl Phys Lett* 93:182901
29. Kittel C (1946) *Phys Rev* 70:965
30. Ginzburg VL, Gorbatshevich AA, Kopayev YV, Volkov BA (1984) *Solid State Commun* 50(4):339
31. Harrison RJ, Dunin-Borkowski RE, Putnis A (2002) *Proc Natl Acad Sci USA* 99:16556
32. Baroni S, de Gironcoli S, Corso AD, Giannozzi P (2001) *Rev Mod Phys* 73:515
33. Gonze X, Lee C (1997) *Phys Rev B* 55:10355
34. Giustino F, Pasquarello A (2005) *Phys Rev B* 71:144104
35. Hamel S, Williamson AJ, Wilson HF, Gygi F, Galli G, Ratner E, Wack D (2008) *Appl Phys Lett* 92:043115
36. Nakamura J, Ishihara S, Natori A, Shimizu T, Natori K (2006) *J Appl Phys* 99:054309
37. Nakamura K, Natori J (2006) *Appl Phys Lett* 89:053118
38. Ramprasad R, Shi N (2005) *Phys Rev B* 72:052107
39. Shi N, Ramprasad R (2005) *Appl Phys Lett* 87:262102
40. Shi N, Ramprasad R (2006) *Phys Rev B* 74:045318
41. Yu L, Ranjan V, Nardelli MB, Bernholc J (2009) *Phys Rev B* 80:165432
42. Pham TA, Li T, Shankar S, Gygi F, Galli G (2011) *Phys Rev B* 84:045308
43. Stengel M, Spaldin NA (2007) *Phys Rev B* 75:205121
44. Stengel M, Vanderbilt D, Spaldin NA (2009) *Nat Mater* 8:392
45. Hohenberg P, Kohn W (1964) *Phys Rev* 136:B864
46. Kohn W, Sham L (1965) *Phys Rev* 140:A1133
47. Kresse G, Hafner J (1996) *J Phys Rev B* 47:558
48. Kresse G, Furthmüller J (1996) *J Phys Rev B* 54:11169
49. Blöchl PE (1994) *Phys Rev B* 50:17953
50. Kresse G, Joubert D (1999) *Phys Rev B* 59:1758
51. Ceperley DM, Alder BJ (1980) *Phys Rev Lett* 45:566
52. Wu Z, Cohen RE, Singh DJ (2004) *Phys Rev B* 70:104112
53. Monkhorst HJ, Pack JD (1976) *Phys Rev B* 13:5188
54. Nelmes RJ, Kuhs WF (1985) *Solid State Commun* 54:721
55. Choy TC (1999) *Effective medium theory: principles and applications*. Oxford University Press Inc., Oxford
56. Osborn JA (1945) *Phys Rev* 67:351
57. Stoner EC (1945) *Phil Mag* 36:803
58. Landau LD, Lifshitz EM, Pitaevskii LP (1984) *Electrodynamics of continuous media, second edition: vol 8 course of theoretical physics*. Pergamon Press, Oxford
59. Burns G, Dacol FH, Remeika JP, Taylor W (1982) *Phys Rev B* 26:2707
60. Kleemann W, Schäfer FJ, Rytz D (1986) *Phys Rev B* 34:7873
61. Ghosez Ph, Cockayne E, Waghmare UV, Rabe KM (1999) *Phys Rev B* 60:836
62. Singh S, Remeika JP, Potopowicz JR (1972) *Appl Phys Lett* 20:135
63. Frey R A, Silberman E (1976) *Helv Phys Acta* 49:1
64. Fontana MD, Idrissi H, Kugel GE, Wojcik K (1991) *J Phys: Condens Matter* 3:8695
65. Foster CM, Li Z, Grimsditch M, Chan S-K, Lam DJ (1993) *Phys Rev B* 48:10160